JOURNAL OF THE AMERICAN WATER RESOURCES ASSOCIATION
Vol. 58, No. 6 AMERICAN WATER RESOURCES ASSOCIATION December 2022

# Mechanisms Controlling Climate Warming Impact on the Occurrence of Hypoxia in Chesapeake Bay

*Richard Tian, Carl F. Cerco, Gopal Bhatt, Lewis C. Linker, and Gary W. Shenk*

**Research Impact Statement**: This paper reports findings on the mechanisms determining climate warming effects on hypoxia and water quality in estuaries and provides important information for mitigation decision-making.

ABSTRACT: Climate change represents an increasing stressor on estuarine and coastal ecosystems. A series of simulations were run using the Integrated Compartment Water Quality Model to determine the magnitude of various mechanisms controlling the effect of climate warming on dissolved oxygen (DO) in the Chesapeake Bay. The results suggested that the average hypoxic volume in the summer would increase by 9% (410 $Mm^3$) from 1995 to 2025 as air temperature increases by 1.06°C and water temperature by 0.9°C. The change in DO solubility contributes 55% of the total climate warming effect, biological rates 33%, and stratification 11%. The Rappahannock Shoal, a hydraulic control point, plays a major role in determining the effect of climate warming on DO in the Bay. Due to the abrupt change in bathymetry, the convergence between seaward-moving freshwater and landward-moving saltwater causes downwelling and enhanced vertical mixing which introduces surface water of higher temperature to the deep channel and accelerates organic matter remineralization and oxygen consumption in deep waters. Surface water DO concentrations will decrease under climate warming conditions due to lower DO solubility, reducing DO flux to the deep channel and contributing to hypoxia development. These findings provide critical information for future management decision making regarding the effects of climate warming on DO in Chesapeake Bay and other estuaries.

(KEYWORDS: Chesapeake Bay; climate warming; modeling; water quality; hydraulic control.)

## INTRODUCTION

Increasing temperatures related to climate change are well documented (IPCC 2013). General Circulation Models (GCMs) project that the global surface temperature will increase by 3.7°C by the end of the 21st Century under the RCP8.5 scenario (RCP: Representative Concentration Pathway) and by 1.8°C under RCP4.5 compared to 1995 (IPCC 2013). The sea surface temperature (SST) over the Northeastern Continental Shelf (ranging from Maine through Maryland) increased about 0.9°C over the last three decades (Thomas et al. 2017; Dupigny-Giroux et al. 2018). Climate warming can represent an increasing stressor on estuarine and coastal ecosystems, particularly for those which experience anthropogenic stress of eutrophication and hypoxia (Justic et al. 1997; Diaz and Breitburg 2009; Meire et al. 2013; Altieri and Gedan 2015; Lehrter et al. 2017).

Chesapeake Bay is the largest estuary in the United States (U.S.). It is located in the states of

Paper No. JAWR-20-0070-P of the *Journal of the American Water Resources Association* (JAWR). Received June 12, 2020; accepted January 31, 2021. 

University of Maryland Center for Environmental Science (Tian), Chesapeake Bay Program Office Annapolis, Maryland,; Attain Inc. (Cerco), Chesapeake Bay Program Office Annapolis, Maryland,; Pennsylvania State University (Bhatt), Chesapeake Bay Program Office Annapolis, Maryland,; USEPA (Linker), Chesapeake Bay Program Office Annapolis, Maryland,; and USGS (Shenk), Chesapeake Bay Program Office Annapolis, Maryland, USA (Correspondence to Tian: rtian@chesapeakebay.net).

*Citation*: Tian, R., C.F. Cerco, G. Bhatt, L.C. Linker, and G.W. Shenk. 2022. "Mechanisms Controlling Climate Warming Impact on the Occurrence of Hypoxia in Chesapeake Bay." *Journal of the American Water Resources Association* 58 (6): 855–875. https://doi.org/10.1111/1752-1688.12907.

Maryland and Virginia with a watershed encompassing parts of six states plus all of Washington, D.C. Chesapeake Bay is eutrophic and experiences hypoxia during the summer season which will most likely be amplified by climate change (Du et al. 2018). Najjar et al. (2010) predicted that climate change will degrade water quality due to increases in precipitation and nutrient loading and decreases in dissolved oxygen (DO) solubility. Irby et al. (2018) predicted that climate change will have an overall detrimental effect in terms of water quality and hypoxia in the Bay mostly due to the change in DO solubility, and Li et al. (2015) also stated the importance of temperature-regulated solubility in determining climate warming effect on DO concentration. However, the question as to how the changing solubility affects DO concentration at the bottom of the stratified Bay remains poorly understood. Stratification is most evident in the Chesapeake in the summer due to a strong thermocline and halocline with warmer fresher water in the surface layer and relatively colder saltier water in deeper layers. DO concentrations are typically below saturation in deeper areas where it is unlikely that reaeration can directly affect DO concentration. Understanding the drivers and mechanisms controlling climate-warming impacts on DO and quantifying their relative importance are critical for adaptive management to mitigate its detrimental effects (Preston 2004). Though this paper is focused solely on the warming aspects of climate change, note that sea level rise and changes in nutrient loading will have additional impacts on DO described in Linker et al. (This volume).

Hydraulic control has been found in Chesapeake Bay where the bathymetry changes abruptly (Maryland Sea Grant College 2004; Zhong and Li 2006; Scully 2016). The Rappahannock Shoal, located in the lower Bay at the mouth of the Rappahannock River, is an area where the deep channel of the central Bay shoals from about 30 to 13 m deep in a very short distance (see bathymetry in Figure 1). Due to the shallow depth, fresher water moving southward meets saltier water moving northward from the coastal ocean, creating a convergence zone where downwelling and strong vertical mixing occur. Due to the physical convergence and turbulence, biogeochemical processes are also intensified at these hydraulic control points (Maryland Sea Grant College 2004). Using conductivity, temperature, and pressure sensors, and acoustic Doppler current profilers, Scully (2016) was able to observe the physical characteristics of the frontal zone at the Rappahannock Shoal in the summers of 2011 and 2013. The shoal is characterized by sharp horizontal salinity gradients across the edge of the shoal and surface water with higher DO is entrained into the deeper layers. The entrained water with higher DO propagates up-estuary along the deep channel with a speed of about 0.08 m/s (Scully 2016).

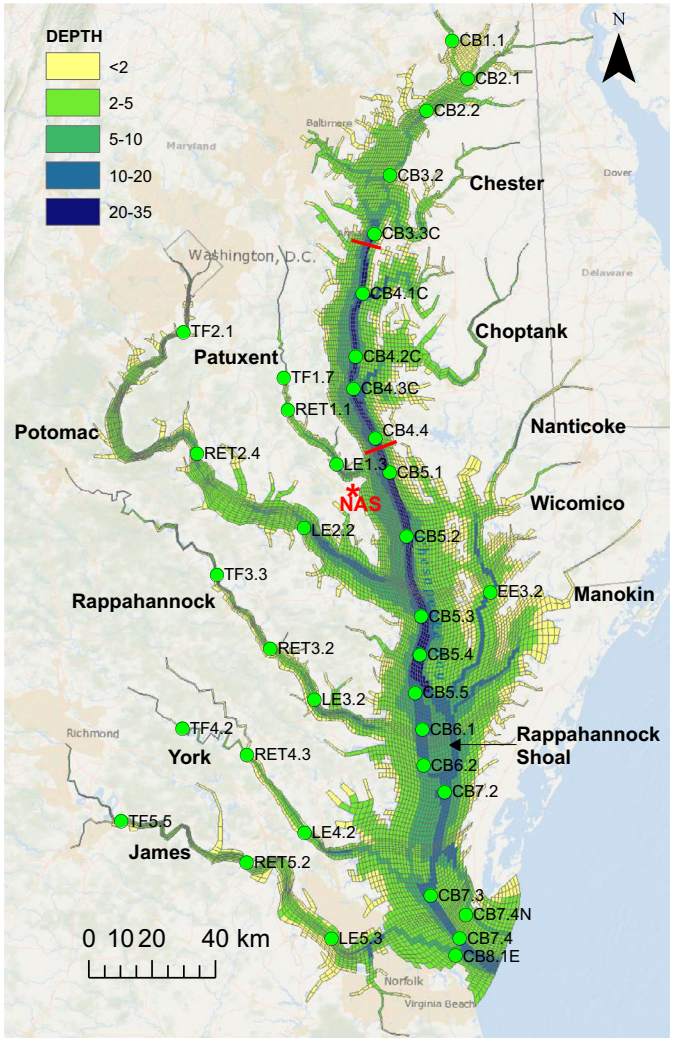


FIGURE 1. Chesapeake Bay, simulation grid, bathymetry (m), tributaries, and observation stations for model calibration. The red star is the Naval Air Station (NAS) from which surface forcing data were collected. Red lines are the boundary of the central segment CB4MH spanning from the mouth of the Chester River to the north to the mouth of the Patuxent River to the south.

The objective of this paper was to assess the effect of the Rappahannock Shoal hydraulic control in determining the climate warming impact on DO in Chesapeake Bay using numerical simulation. Surface water entrained to the deep channel will have a higher temperature and lower DO solubility under warming conditions. The higher water temperature will increase the remineralization rate and hypoxia development. In addition, the lower DO solubility of the warmer entrained water will lower DO concentration, reducing DO supply to the deep channel and further aggravating hypoxia development.

We conducted a series of model simulations under warming climate conditions and compared the results with the control run using the Curvilinear Hydrodynamic Model in 3D (CH3D)-Integrated Compartment Model (ICM) simulation platform. Model scenarios were designed to discern each mechanism controlling climate-warming effects on hypoxia and water quality in the Bay, including DO solubility, respiration rate, and stratification. The CH3D (Sheng and Hirsh 1984; Sheng 1990; Johnson et al. 1991; Sheng et al. 1991) simulates the physical fields of currents and turbulence diffusivity which are used to drive the ICM (Cerco and Cole 1993; Cerco and Noel 2004, 2013). ICM simulates water quality, including phytoplankton, chlorophyll, nutrients, organic substances, DO, and sediment diagenesis. This simulation system has been used by the Chesapeake Bay Program in supporting management decision making by the Bay Partnership and the development of the Total Maximum Daily Load (TMDL). Also, ICM has been successfully applied in Chesapeake Bay using an unstructured grid (Xia and Jiang 2016).

## METHODS

### *Model*

Model simulations were carried out using the integrated hydrodynamic-water quality model CH3D-ICM (Cerco and Cole 1993; Cerco and Noel 2013). CH3D and ICM share the same 3D model grid structure and surface meteorological forcing. The major characteristics of CH3D and ICM related to temperature and heat flux are briefly described below. CH3D uses a curvilinear orthogonal grid in the horizontal and a $z$-coordinate in the vertical, with 11,064 surface cells ranging from 200 m to 1 km in resolution. The surface layer is 2.13 m thick at mean tide and varies in thickness due to meteorological and tidal forcing. All layers below have a constant thickness of 1.523 m. The number of vertical layers changes with the bathymetry, ranging from 19 layers in the deep central Bay to 1 layer in the shallow coastal region. CH3D computes the current and turbulence diffusivity that are used to drive the ICM simulation. ICM has a flexible model structure with a maximum of 36 state variables, but any of the variables can be disabled during the simulation. In this application, 28 variables were activated: temperature, salinity, three groups of phytoplankton (cyanobacteria, diatom, and green algae, with the latter representing all other species than the two former groups), nutrients (nitrogen and phosphorus), dissolved and particulate organic matter, DO, chemical oxygen demand (COD), and suspended sediments. Phytoplankton growth is controlled by light availability, nutrient limitation, and temperature. The temperature control on phytoplankton growth is parameterized using the function (Cerco and Noel 2013):

$$\mu(T) = \mu_{\max} \cdot e^{-K_T(T-T_o)^2}, \quad (1)$$

where $\mu_{\max}$ is the maximum growth rate, $K_T$ is an exponential coefficient for temperature forcing on phytoplankton growth, and $T_o$ is the optimal temperature. The optimal temperature $T_o$ is set to 37°C for green algae. It should not be interpreted as the optimal temperature for a specific species of phytoplankton, but rather the optimal value for the population represented by the variable. $K_T$ is set to 0.002°C$^{-1}$ and $\mu_{\max}$ to 300 g C/gchl/day based on Cerco and Noel (2013). Phytoplankton respiration and mineralization are parameterized with the exponential function:

$$R = a_R e^{-k_R(T-T_R)}, \quad (2)$$

where $a_R$ is the respiration rate set to 0.03 day$^{-1}$ at the reference temperature $T_R$ (20°C) and $k_R$ is the exponential coefficient set to 0.032 (Cerco and Noel 2013).

DO solubility ($DO_S$) is computed using the Garcia and Gordon formulation (Garcia and Gordon 1992). DO solubility in pure water (salinity = 0) decreases from 14.2 mg/L at 1°C to 6.9 mg/L at 35°C, i.e. DO solubility is reduced by half within the commonly observed water temperature range in the Bay (Figure 2). The relationship between DO solubility and temperature is nonlinear and the slope is greater at the lower temperature range than at higher temperature. The slope in pure water is about −0.25 mg/L/°C at 5°C, −0.21 mg/L/°C at 15°C, −0.15 mg/L/°C at 25°C and −0.11 mg/L/°C at 35°C. Higher salinity results in lower DO solubility. DO solubility decreases by 2.7 mg/L from pure water (salinity = 0) to salt water of 30 psu at the water temperature of 1°C, and this difference is reduced to 1.0 mg/L at 35°C water temperature over the same range of salinity change.

ICM uses the DiToro-Fitzpatrick diagenesis model to simulate the flux of organic matter to the bottom sediment and the remineralization, burial, and flux of nutrients and COD from the sediment to the water column (DiToro and Fitzpatrick 1993). Two sediment layers (aerobic and anaerobic) are simulated, and organic substances are divided into three categories based on the rate of remineralization (Westrich and Berner 1984) as $G_1$, $G_2$, and $G_3$. $G_1$ is labile, $G_2$ is more refractory, and $G_3$ is nearly inert. Linear approaches are implemented in terms of decay from organic particulate substances to dissolved inorganic components and the decay rates are linked to temperature using the formula (Cerco and Noel 2004):

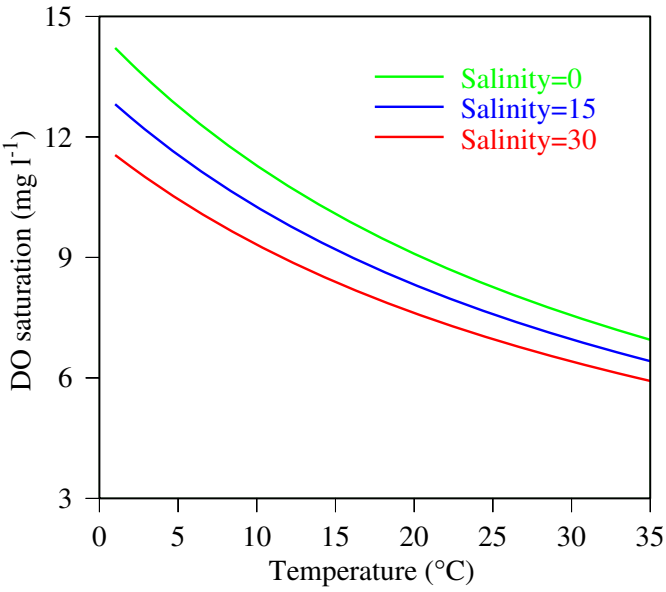


FIGURE 2. Dissolved oxygen (DO) saturation in function with water temperature and salinity.

$$\frac{\partial Gi_i}{\partial t} = K_{Gi} G_i \theta_i^{(T-20)}, \tag{3}$$

where $G_i$ are the particulate organic matter categories $G_1$ to $G_3$, $K_{Gi}$ is the decay rate at the reference temperature of 20°C, and assigned to $3.5 \times 10^{-2}$ day$^{-1}$ for $G_1$, $1.8 \times 10^{-3}$ day$^{-1}$ to $G_2$ and $6.5 \times 10^{-5}$ day$^{-1}$ to $G_3$, which yield half-life spans of 20 days, 1 year, and 30 years, respectively, and $\theta_i$ is the parameter determining the relationship between the decay rate and temperature (1.1, 1.15, and 1.17 for $G_1$, $G_2$, and $G_3$, respectively).

Edinger et al. (1974) deduced an equation for equilibrium water temperature ($T_e$) with the atmosphere:

$$T_e = \frac{H_{sn} + H_{an} - 306 + (K_T - 4.48) T_d^*}{K_T + 0.05 T_d^* - 0.025 T_e}, \tag{4}$$

Where:

$$K_T = 4.48 + (\beta + 0.47) f(W) + 0.05 T_e, \tag{5}$$

$$f(W) = 9.2 + 0.46 W^2, \tag{6}$$

$$T_d^* = T_d + \frac{0.47 (T_a - T_d)}{\beta + 0.47}, \tag{7}$$

$$\beta = 0.35 + 0.015 \frac{T_e + T_d}{2} + 0.0012 \frac{(T_e + T_d)^2}{4}. \tag{8}$$

$H_{sn}$ and $H_{an}$ are net solar radiation and net atmospheric long-wave radiation, $K_T$ is the heat-transfer coefficient between the atmosphere and the ocean, $W$ is the wind speed at 7 m above the sea surface in m/s, $T_a$ air temperature, and $T_d$ dew point. Equations (4 through 8) were run iteratively until a steady-state solution is reached and the final solutions were then used during the simulation to calculate the heat flux $H_{net}$ in watt m$^{-2}$:

$$H_{net} = K_T (T_e - T_s), \tag{9}$$

where $T_s$ is surface water temperature. The same heat flux scheme (Equation 9) was applied to both CH3D and ICM.

### *Forcing Data*

The surface forcing data, including air temperature, relative humidity, dew point, cloudiness, and wind are from the Naval Air Station located at the Patuxent River mouth (USW00013721; 38.286N, −76.412W; Figure 1). Nutrient and sediment loadings were generated by using the Chesapeake Bay Program partnership watershed model (Chesapeake Bay Program 2017). All the sensitivity analysis scenarios presented in this paper share the same nutrient loads of the calibration (control) scenario, representing historical meteorological, watershed, and management conditions from 1991 to 2000. The annual average loading of total nitrogen to the Chesapeake Bay is about $146 \times 10^6$ kg and $10 \times 10^6$ kg of total phosphorus over the simulation period from 1991 to 2000. Open boundary conditions at the Bay mouth were based on linear interpolation of biweekly observations.

To simulate the effects of climate warming, the projected change in air temperatures was added to the observed $T_a$ in Equations (4–8) and the $T_e$, $K_T$, and $H_{net}$ were re-computed through the iterative procedure. Statistically downscaled projections using the Bias Corrected Spatial Disaggregation method for 31 GCMs included in Coupled Model Intercomparison Project Phase 5, CMIP5 (Taylor et al. 2011; IPCC 2013) were used. The GCMs were developed by research organizations from various countries over the world, including seven from U.S., four each from China, France, and Japan, three from Australia and Brazil, two from Germany and Norway, and one from the European Union, Canada, and Russia (Table 1). The monthly median of the ensemble projection from these 31 GCMs under the RCP4.5 scenario has been used in this study. The ensemble analysis provided county scale monthly air temperature change over the 30-year period between 2025 and 1995 (Chesapeake Bay Program 2020). Data collected at the Naval Air Station at the Patuxent River Mouth were

used to drive the ICM simulation for the control scenario. This station is located at the boundary between Calvert and St. Mary's counties in Maryland. Consequently, the average of the projected change in temperature between these two counties was used for the climate change scenarios. This analysis showed that the average monthly air temperature was projected to increase by about 0.92°C in February to as high as 1.22°C in December over the 30 years from 1995 to 2025, with an annual average increase of about 1.06°C (Chesapeake Bay Program 2020).

At the open boundary connecting to the coastal and continental shelf waters, Thomas et al. (2017) and Dupigny-Giroux et al. (2018) conducted extensive analyses on historical data of SST on the Northeastern U.S. Continental Shelf and the Mid-Atlantic Bight to estimate the change in observed water temperature over multiple decades. Thomas et al. (2017) reported that SST increased 0.3°C per decade from 1982 to 2014, which is equivalent to 0.9°C over 30 years. Similarly, Dupigny-Giroux et al. (2018) estimated that SST increased 0.033°C per year from 1982 to 2016, which yields a 0.99°C increase over 30 years. Based on these studies, water temperature change at the open boundary was linked to the air temperature change by a factor of 0.9 for the surface layer, which yields an increase of 0.95°C over 30 years. Water column temperatures at the open boundary for the control scenario were based on field measurements at the

TABLE 1. General Circulation Models included in the ensemble downscale analysis (from IPCC 2013).

| Model | Origin | Country |
|---|---|---|
| ACCESS1-0 | Commonwealth Scientific and Industrial Research Organization and Bureau of Meteorology | Australia |
| BCC-CSM1-1 | Beijing Climate Center, China Meteorological Administration | China |
| BCC-CSM1-1-M | | China |
| CanESM2 | Canadian Centre for Climate Modelling and Analysis | Canada |
| CCSM4 | National Center for Atmospheric Research | U.S. |
| CESM1-BGC | Community Earth System Model Contributors | U.S. |
| CESM1-CAM5 | | U.S. |
| CMCC-CM | Centro Euro-Mediterraneo per I Cambiamenti Climatici | EU |
| CNRM-CM5 | Centre National de Recherches Météorologiques/Centre Européen de Recherche et Formation Avancée en Calcul Scientifique | France |
| CSIRO-Mk3-6-0 | Commonwealth Scientific and Industrial Research Organization, Queensland Climate Change Centre of Excellence | Australia |
| FGOALS-g2 | Laboratory of Numerical Modeling for Atmospheric Sciences and Geophysical Fluid Dynamics, Institute of Atmospheric Physics, Chinese Academy of Sciences, and Center for Earth System Science, Tsinghua University | China |
| FIO-ESM | The First Institute of Oceanography, State Oceanic Administration, China | China |
| GFDL-CM3 | NOAA Geophysical Fluid Dynamics Laboratory | U.S. |
| GFDL-ESM2G | | U.S. |
| GFDL-ESM2M | | U.S. |
| GISS-E2-R | NASA Goddard Institute for Space Studies | U.S. |
| HadGEM2-AO | Met Office Hadley Centre (additional HadGEM2ES realizations contributed by Instituto Nacional de Pesquisas Espaciais) | Brazil |
| HadGEM2-CC | | Brazil |
| HadGEM2-ES | | Brazil |
| INM-CM4 | Institute for Numerical Mathematics | Russia |
| IPSL-CM5A-LR | Institut Pierre-Simon Laplace | France |
| IPSL-CM5A-MR | | France |
| IPSL-CM5B-LR | | France |
| MIROC-ESM | Japan Agency for Marine-Earth Science and Technology, Atmosphere and Ocean Research Institute (The University of Tokyo), and National Institute for Environmental Studies | Japan |
| MIROC-ESMCHEM | | Japan |
| MIROC5 | Atmosphere and Ocean Research Institute (The University of Tokyo), National Institute for Environmental Studies, and Japan Agency for Marine-Earth Science and Technology | Japan |
| MPI-ESM-LR | Max-Planck-Institut für Meteorologie (Max Planck Institute for Meteorology) | Germany |
| MPI-ESM-MR | | Germany |
| MRI-CGCM3 | Meteorological Research Institute | Japan |
| NorESM1-M | Norwegian Climate Centre | Norway |
| NorESM1-ME | | Norway |

entrance of the Bay. Temperature change across the water column under future climate change conditions was assumed to co-vary with observed profile and stratification in the open boundary specification as described below under unstratified and stratified conditions. If the water column is well mixed without stratification, water temperature change is the same from the surface to the bottom. Under stratified conditions, water temperature change is proportional to the ratio between the observed water temperature in the water column and the surface water temperature. If the water temperature at a depth is half of the surface temperature, for example, water temperature change under climate change condition is half of the surface temperature change at that depth.

### *Observed Data and Statistical Analysis*

The Chesapeake Bay Program has maintained a monitoring program for the entire Bay since 1984. From a larger monitoring network, 26 stations located in the main stem and the major tributaries were selected for model calibration (Figure 1). Sampling is carried out twice per month from March through October and once per month for the rest of the year. A wide range of physical, biological, and biogeochemical parameters were analyzed, but in this paper only temperature, salinity, DO, and chlorophyll are presented. Time-series data were plotted for the central Bay station CB4.2C, whereas data from all other stations were compared using Taylor and Target Diagrams (Taylor 2001; Jolliff et al. 2009; Tian et al. 2014). Briefly, Taylor diagrams compare the simulation to observations in terms of the correlation coefficient, the standard deviation (std) of both simulated and observed data, and centered root mean squared error (CRMSE) on the same diagram (Taylor 2001). The angle from zero indicates the correlation between simulation and observation and the distance from the origin is the normalized std of the simulated values (simulation std divided by observation std), with the result that the overall distance between data and simulation on the Taylor diagram is proportional to the CRMSE.

In the Target diagram, the bias between the simulation mean and the observation mean is scaled on the $y$ axis and the CRMSE (unbiased) on the $x$ axis. As a result, the root mean squared error (RMSE) is the radial distance from the origin to the data point (Jolliff et al. 2009; Tian 2019). As in the Taylor diagram, the bias and RMSE are normalized to the std of the observed data. The combined Taylor and Target diagram can thus give a comprehensive assessment of the simulation by providing the correlation coefficient, std, the CRMSE, the bias, and the total RMSE (see "Results" section for graphic examples).

### *Model Operation*

The model was first spun up with 1991 forcing repeated over 10 years to equilibrate the storages in the model to changes in inputs, then run an additional 10 years from 1991 to 2000 for the analyzed outputs. The period was selected by the Chesapeake Bay Program partnership as a representative hydrologic decade for the Chesapeake Bay TMDL (USEPA 2010; Linker et al. 2013). Five scenarios were simulated: (1) The *control run* using the forcing and nutrient loading representing conditions from 1991 through 2000; (2) the *All factors* scenario which includes all the changes considered in this paper under climate warming conditions: heat flux increase at the sea surface, temperature increase at the open boundary, DO solubility, biological rates, current, turbulence diffusivity, and temperature simulated under climate warming condition; (3) the *DO solubility* scenario in which all forcing files and hydrodynamic fields were kept the same as in the control run, except the DO solubility which was computed using the temperature simulated under climate warming conditions; (4) the *Biological rate* scenario in which all the forcing files were the same as in the control run except biological rates which were recomputed using the temperature simulated under climate warming conditions; and (5) the *Stratification* scenario in which all the forcing files were kept the same as in the control run except the turbulence diffusivity field which was recomputed under climate warming conditions. Changes in the stratification under climate warming condition were reflected in the turbulence diffusivity field, with stronger stratification leading to lower turbulence diffusivity and vice versa.

## RESULTS

### *Observed and Simulated Time-Series Data at the Central Station CB4.2C*

This section compares the outputs of the control run with field measurements to evaluate the model performance and accuracy in reproducing the field observations. Figure 3 depicts the 10-year time series data of temperature, salinity, DO, and chlorophyll at both the surface and bottom layers at Station CB4.2C

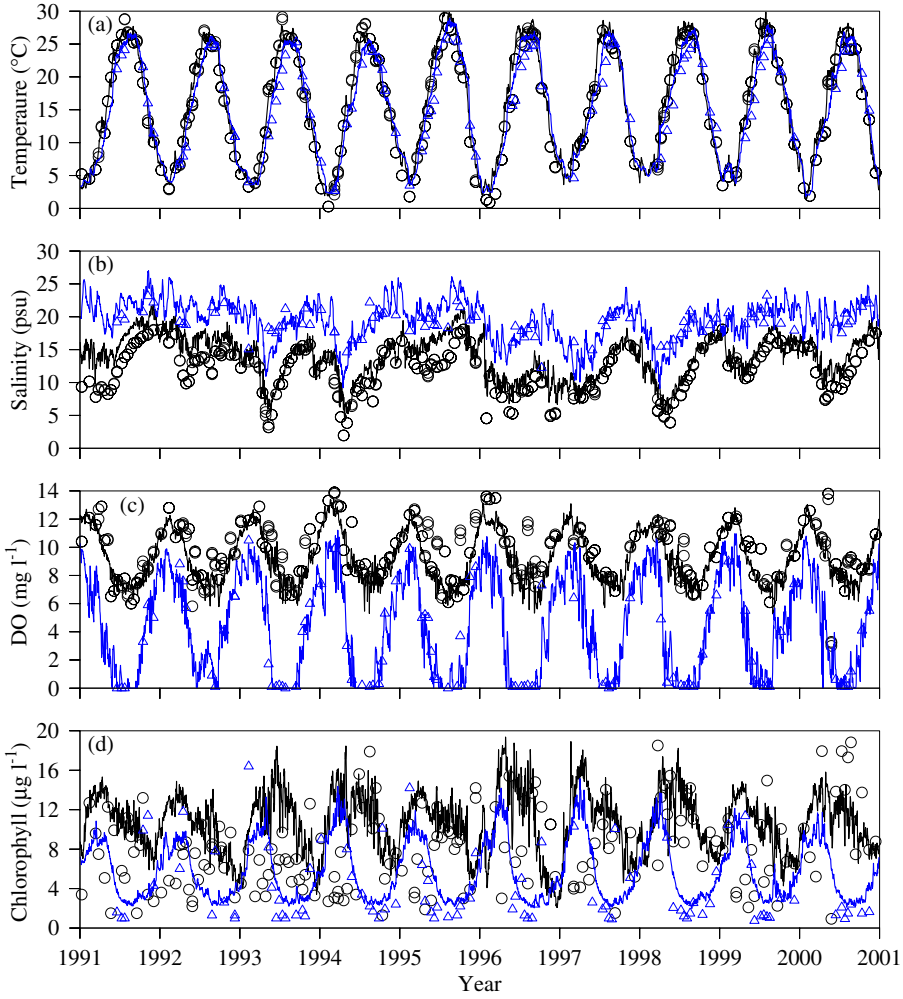


FIGURE 3. Surface (black) and bottom (blue) time-series data of observation (open dots for surface and triangles for bottom) and simulation (continuous lines) at the central station CB4.2C of temperature (a), salinity (b), DO (c), and chlorophyll (d). Simulation results are from the control run.

located in the central Bay where the water depth reaches to 30 m. The temperature simulation matched well with the observations in both seasonal cycles and magnitude (Figure 3a). Water temperature reached up to 30°C in summer and down to near 0°C in winter in both the simulation and observation. There were interannual variations in the temperature time-series data, with temperature reaching up to 30°C in the summer of 1995, but only 26°C in the summer of 1992. Water temperature dropped to 0°C in the winter of 1996, but only to 6°C in 1997. The average temperature in summer was 26.0°C in the surface layer and 25.2°C in the bottom layer, and winter temperatures for the surface and bottom layers were 4.8 and 4.9°C, respectively. The most significant difference was the lag time between bottom and surface layers in spring when the temperature increased in the bottom layer lagged the surface layer by about four weeks.

The salinity simulation matched relatively well with the observations during the entire simulation period (Figure 3b). In contrast to temperature which did not show a significant vertical difference during most of the time, salinity was significantly different between the surface and bottom layers. The long-term average salinity over 10 years was 16 psu in the surface layer and 22 psu in the bottom layer, i.e., a difference of 6 psu. Given the strong halocline with lighter fresher water above heavier saltier water, the pycnocline existed despite the weak thermocline. Seasonal variation of salinity was much smaller than that of temperature. Nonetheless, salinity tended to be lower during spring than in other seasons, indicating freshening during the high river discharge season.

The model successfully reproduced the seasonal variations and differences of DO between the surface and bottom layers (Figure 3c). Hypoxia, defined as DO

<2 mg/L (Zhang et al. 2010; Roman et al. 2019), occurred every summer in the bottom water. It started typically in April and ended in September, a duration of about five months. DO in the surface layer ranged from 6 mg/L in summer to 14 mg/L in early spring. The higher DO concentration in winter and spring was related to increased DO solubility in winter and supersaturation during phytoplankton blooms in spring. Even in winter when vertical mixing was stronger, stratification in DO concentration remained with higher DO in the surface layer than in the bottom layer.

There was high spatial and temporal variability in observed chlorophyll concentrations which were difficult to simulate with similar accuracy as the other variables presented above (Figure 3d). Nonetheless, the magnitude and seasonality were coherent between the two datasets, higher during the spring and summer seasons and lower in winter. The water depth at the central station CB4.2C is 30 m, which is much deeper than the euphotic zone. However, chlorophyll concentration exhibited remarkable seasonal cycles in the bottom layer. Bottom chlorophyll concentration was almost as high as in the surface layer during the spring phytoplankton bloom, indicating a quick transfer of phytoplankton biomass from the surface to the bottom layer through sinking. Summer chlorophyll concentration remained at a relatively high level in the surface layer, but not in the bottom layer. The reduction in chlorophyll concentration in the deep layer was typically contemporaneous with the reduction of DO when bottom water temperature rose above 15°C.

### *Taylor and Target Diagram Comparison between Simulation and Observation*

As mentioned earlier, data from 26 stations were used for model calibration. It is impractical to present all the time-series data for all the stations. Instead, the Taylor and Target diagrams were used to assess the accuracy of the model predictions against observed data for all calibration stations (Figures 4 and 5). Results from the temperature simulation were comparable to measurements for both surface and bottom waters (Figure 4a, 4b for surface water and e and f for bottom water). All of the stations were clustered close to the data (the stars in Figures 4 and 5) on the Taylor diagram and at the center on the Target diagram, which means that there was a high correlation ($r > 0.95$) between the simulation and observation and limited or negligible bias between them (<0.5 of observation std). The comparison between salinity simulation and observation was less robust than temperature, but within a reasonable range in terms of correlation coefficients and CRMSE (Figure 4c, 4d, 4g, 4h). Most of the correlation coefficients between simulation and observations were higher than 0.7, with centered root mean square errors lower than half of the std of the observed data (Figure 4c, 4g). Station CB1.1 located at the Bay head was an outlier, basically without correlation between simulation and measurements. This station is in the tidal fresh zone where salinity was mostly zero and occasionally with a value <0.5 psu. Stations TF1.7, CB7.4, and CB7.4N also had higher CRMSEs than the rest of the stations in the surface layer. TF1.7 is also located in the tidal fresh zone (Figure 1). This suggested that the calibrated CH3D-ICM was robust for the mainstem Bay, but in tidal fresh areas in the tributaries, the simulation was less robust than in the main stem.

DO simulation was also very robust as compared with the observed data (Figure 5a, 5b, 5e, 5f). On the Taylor diagram, the correlation coefficients between simulation and observation were higher than 0.8 for most of the stations with a CRMSE smaller than half of the std of the observation (Figure 5a, 5e). Two stations in the tidal fresh zone, TF2.1 in the Potomac River and TF5.5 in the James River, had a correlation coefficient of approximately 0.6 and a CRMSE within about 1 std of the observation. These two stations were also outliers in the Target diagram (Figure 5b, 5f). Most of the stations had total RMSEs within 1, but Stations TF2.1 and TF5.5 had total RMSEs about 1.5 and 2. Both the bias and the unbiased RMSEs due to variability contributed to the increased total mean squared error.

The chlorophyll simulation was not as robust as the previous variables (Figure 5c, 5d, 5g, 5h). Although the magnitude and seasonality were reproduced by the model (Figure 3d), the correlation coefficients ranged between 0.2 and 0.8 for most of the stations in the surface layer. The bias on the Target diagram was mostly within 1 std of the data, but the unbiased RMSE reached 2–3 times of the std of the observation. The high variability in space and time made it relatively difficult for the model to exactly reproduce the data. However, the magnitude and seasonal variations matched well between model prediction and observation.

### *Temperature Change under Climate Warming Condition*

Average surface water temperature was computed for the 10-year simulation in August, which is generally the warmest month. Average water temperature did not show dramatic spatial variation in the Bay (Figure 6a). The surface water temperature was mostly about 27°C. Only two areas showed significant anomaly, the Bay mouth where the surface water

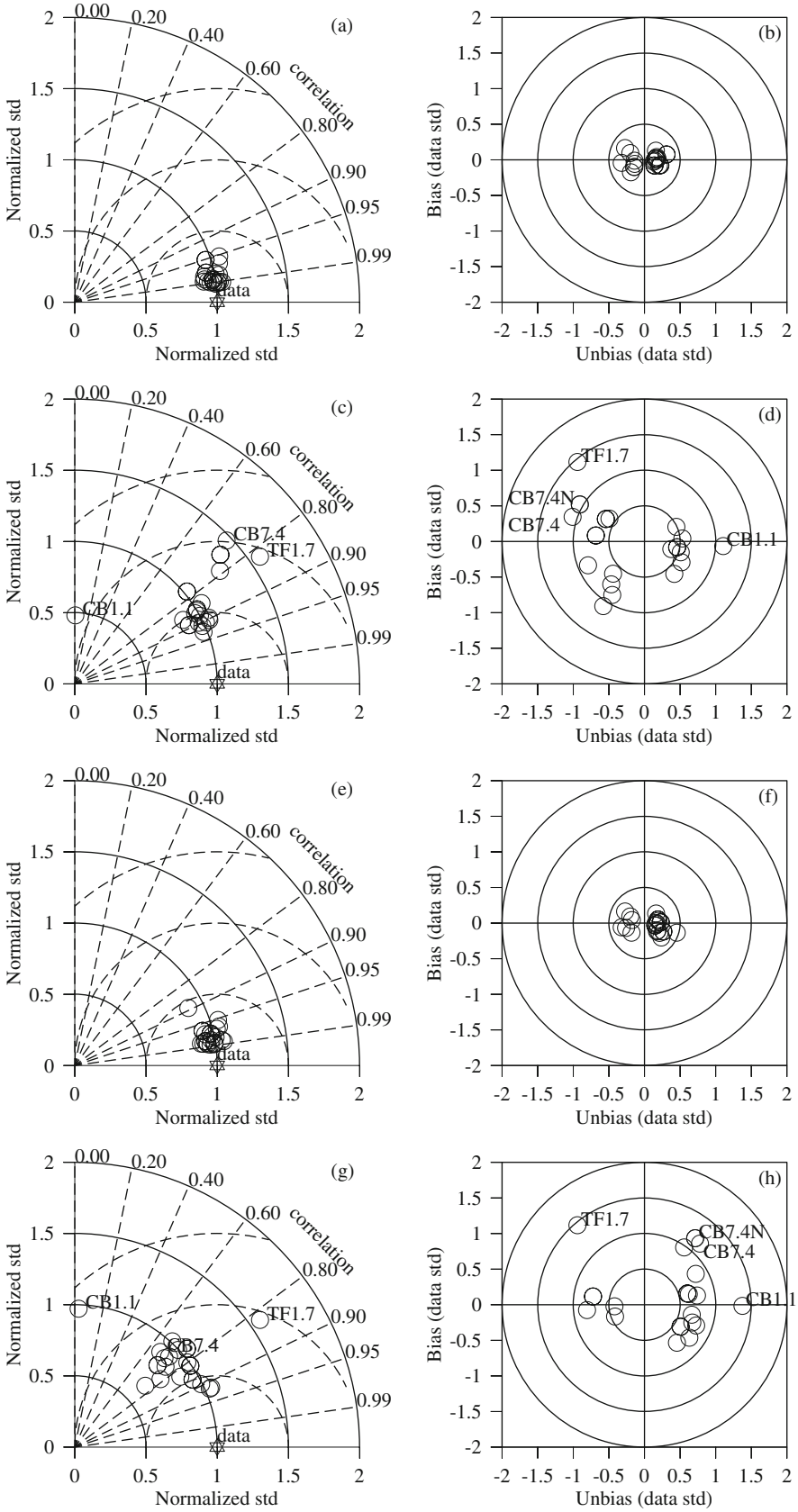


FIGURE 4. Taylor (left) and Target (right) diagrams for surface temperature (a,b) and salinity (c,d) and bottom temperature (e,f) and salinity (g,h) between the control simulation and observation at the calibration stations. Bias is the difference of mean between simulation and observation and unbias is the centered root mean squared error.

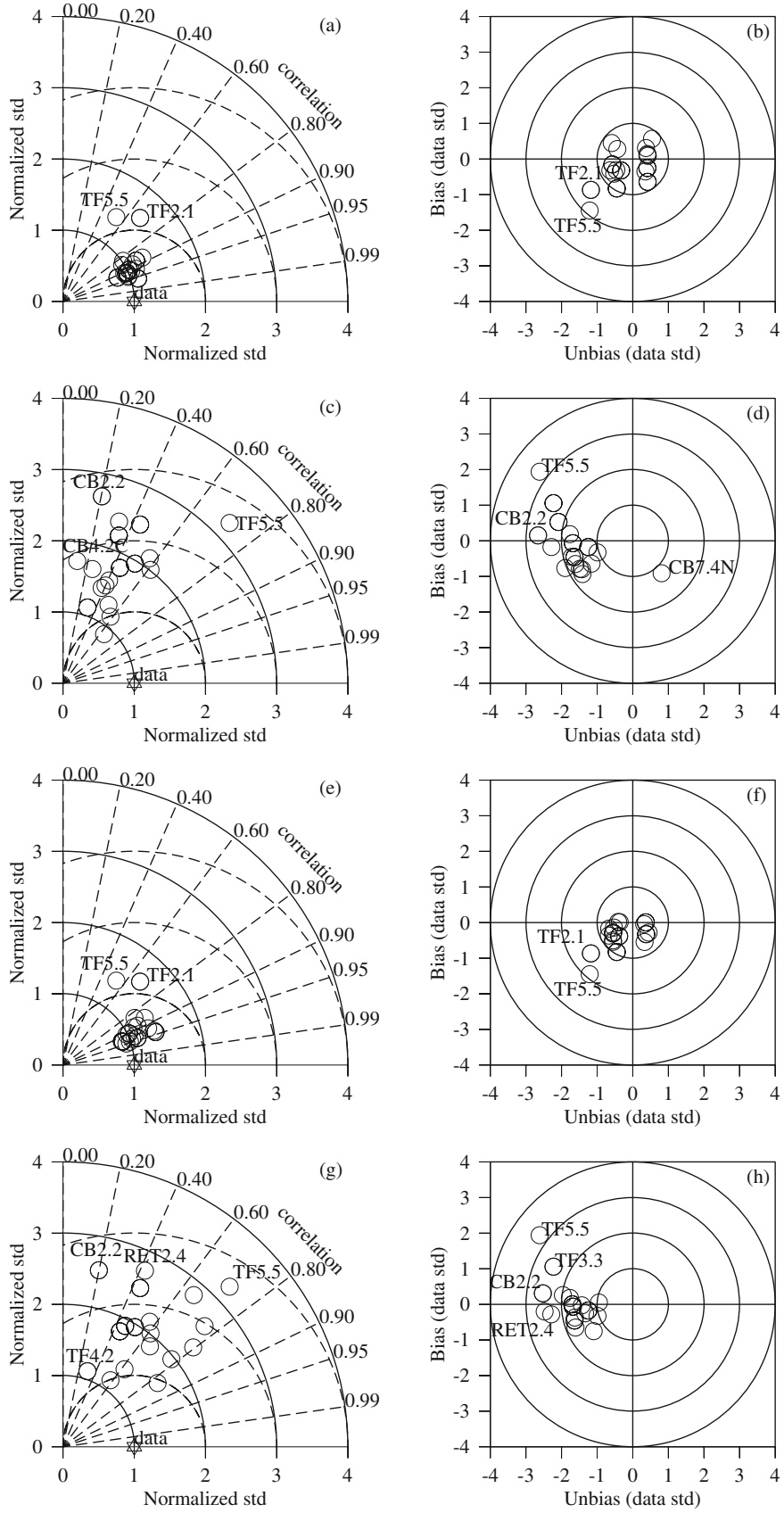


FIGURE 5. Taylor (left) and Target (right) diagram for surface DO (a,b) and chlorophyll (c,d), and bottom DO (e,f), and chlorophyll (g,h) between the control simulation and observation at the calibration stations.

temperature was about 2°C lower and the eastern side of the lower Bay where temperature was about 1°C higher than the rest of the Bay. Similar patterns at the mouth and eastern side were simulated in the bottom layer (Figure 6b). Additionally, the bottom temperature in the main stem was slightly lower than in the shallow regions, but the difference was mostly within 1°C. Water temperature change with climate warming was mostly within the range from 0.7°C to 1.0°C (Figure 6c, 6d). Overall water temperatures increased less in the main stem than in the shallow areas and surface water temperature tended

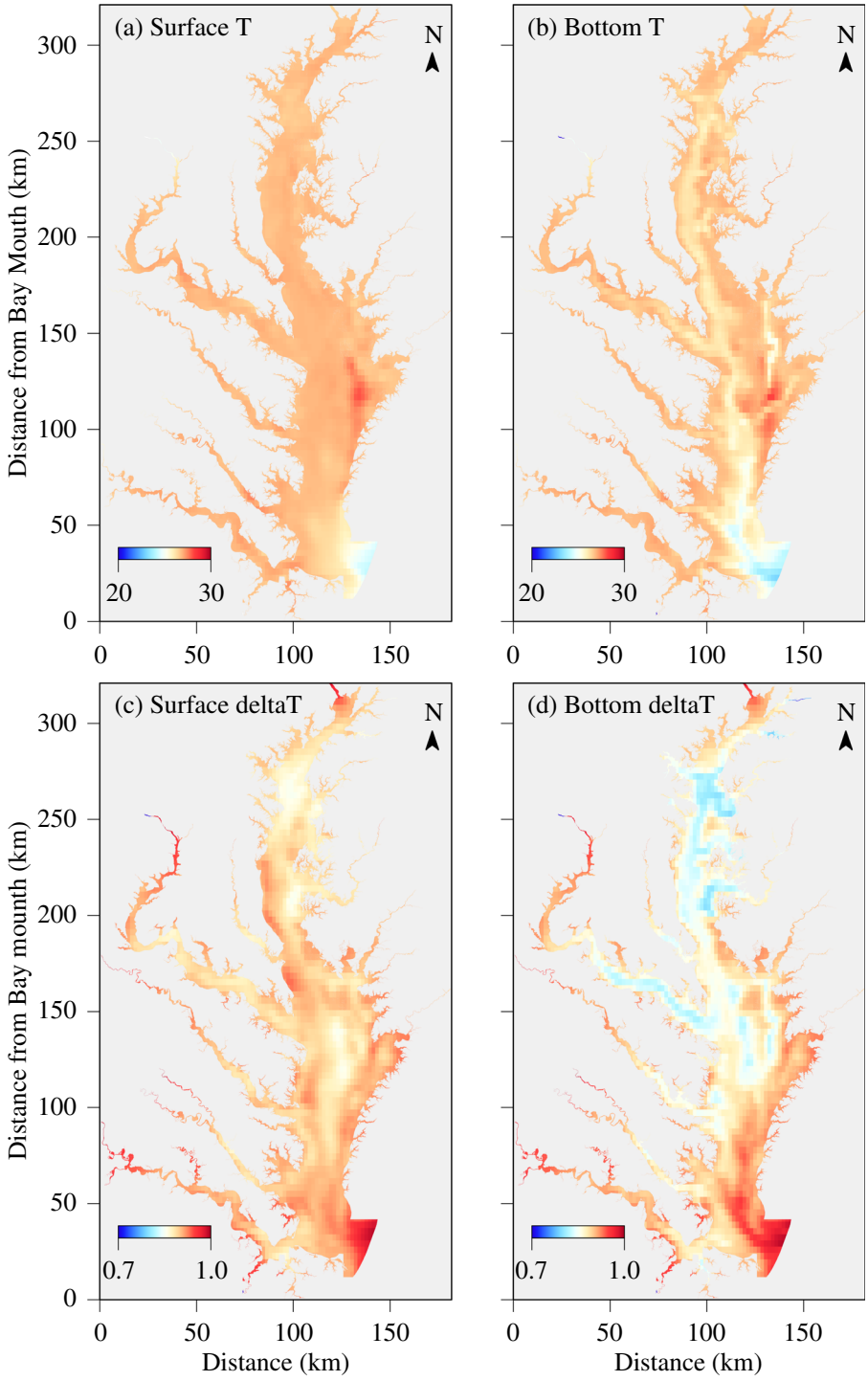


FIGURE 6. Temperature (°C) in the surface (a) and bottom (b) layers of the control run and temperature change in the surface (c) and bottom (d) layers between the All factors combined run and the control run (average in August from 1991 to 2000).

to increase more than in the bottom layer. Also, the temperature change appeared higher at the mouth of the Bay, but this signal did not widely spread into the interior of the Bay.

Along the main stem of the Bay, surface water temperature increased by 0.85°C to 0.94°C in summer (June through September) and bottom water temperature by 0.77°C to 0.96°C (Figure 7). At the station CB2.1 at the Bay head and at the lower Bay from Station CB6.2 on the Rappahannock Shoal to the Bay mouth, water temperature increased under climate warming conditions was practically the same in the surface and bottom layers. In the main stem of the Bay from Station CB3.2 to CB5.5, surface water temperature increased more than bottom water temperature. Surface water temperature increased about 0.92°C and bottom water by 0.85°C. At Station CB3.2 in the upper Bay, temperature change was the lowest among all the main stem stations, by 0.85°C in the surface and 0.77 at the bottom. This was also noticeable in the spatial distribution (Figure 6c, 6d) in which there was an area in the upper Bay where temperature change was lower as compared to the rest of the Bay. Overall, the differences in water temperature change under warming climate were limited along the Bay and between the surface and bottom layers, mostly within 10%.

As a comparison with field observations, the long-term trend of measured surface water temperature from 1984 to 2016 at the central Bay station CB4.2C showed a slope of 0.0346°C per year, which yields a 30-year increase of about 1°C in the surface layer, and 0.9°C in the bottom layers (Figure 8). These numbers were quite comparable to the simulated results of temperature increase over 30 years, with a difference <10%. As mentioned earlier, data analysis in the coastal region also generated a similar magnitude of temperature increase over 30 years (Thomas et al. 2017; Dupigny-Giroux et al. 2018).

### *Bottom DO Change under Climate Warming Condition*

The bottom DO concentration in the control run (Figure 9a) and bottom DO concentration change under climate warming conditions (Figure 9b) for August averaged over 10 years were from the bottom model cells in the simulation domain. Given that the bottom cells were at different depths based on the bathymetry of the Bay, the mapped values were not at the same depth. Hypoxia, defined here as DO <2.0 mg/L, occurred in the deep channel in the central part of the Bay, with only limited occurrence on the eastern tributaries (Figure 9a). DO decreased practically in the entire model domain in the simulation with climate warming condition compared to the control run (Figure 9b). Only at the Bay mouth was DO concentration similar in both climate warming and control run simulations, which most likely resulted from the same specified DO concentration at the open boundary. In the main stem of the Bay and in the lower estuaries of all the tributaries, bottom DO concentrations decreased in spatial average by about 0.2 ± 0.06 mg/L from the control run to the climate warming simulation. On the Eastern Shore in the mid-Bay and in the tidal fresh zone of the tributaries, DO concentration decreased up to 0.3 ± 0.07 mg/L.

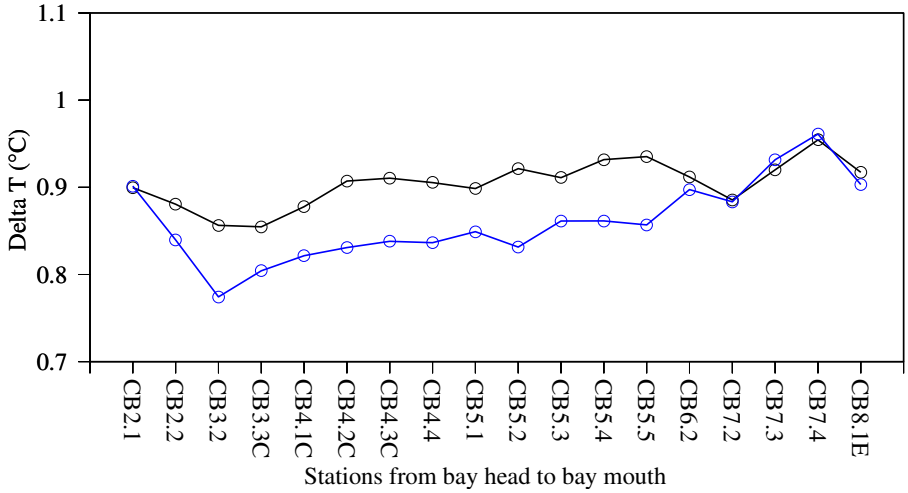


FIGURE 7. Summer (June–September) water temperature change (delta *T*) under 2025 climate warming condition (CWC) from the control run. Black: Surface water temperature change along the main stem stations; Blue: Bottom water temperature change along the main stem stations.

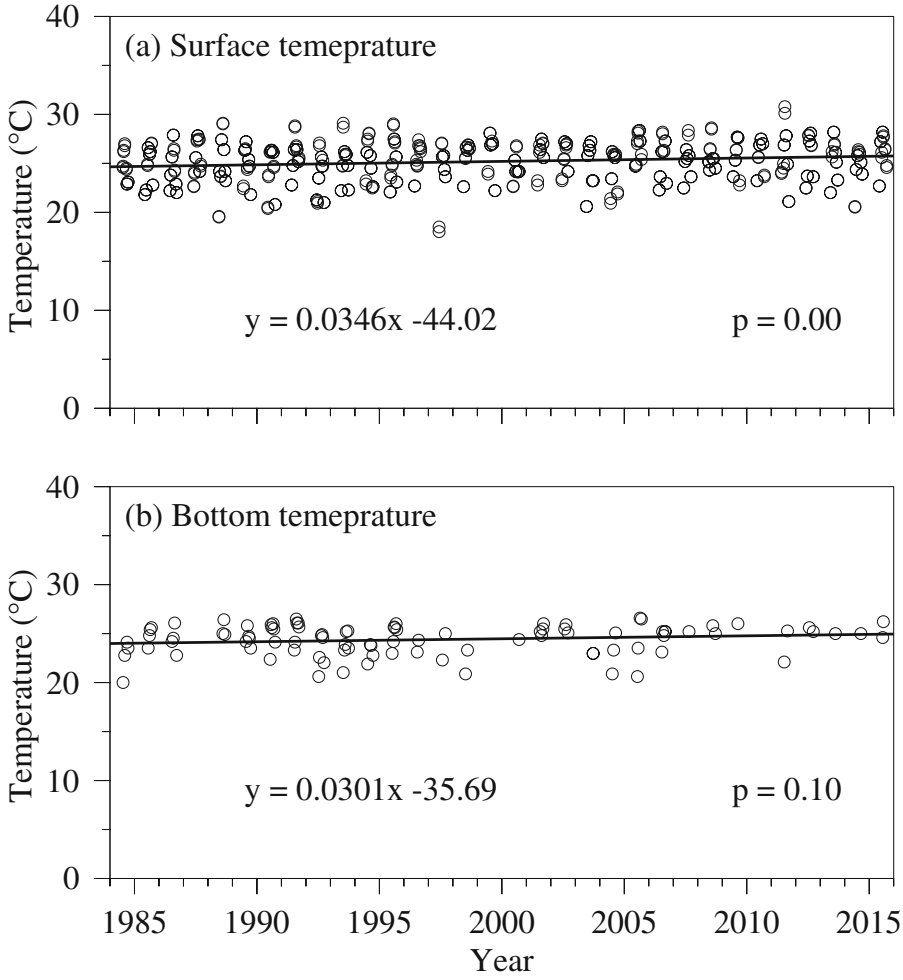


FIGURE 8. Observed surface (a) and bottom (b) temperature trend in summer (June–September) over 32 years from 1984 to 2016 at the central station CB4.2C.

*Simulated Hypoxic Volume in the Bay*

Hypoxia is defined here as DO concentration below 2 mg/L (Zhang et al. 2010; Roman et al. 2019). The average daily hypoxic volume in summer (June through September) over the 10 simulated years was 4.57 $km^3$ in the whole Bay and increased to 4.98 $km^3$ in the climate-warming scenario with all factors included (Figure 10). As mentioned in the Methods section, the DO solubility decreases with increasing water temperature and a 1°C increase in water temperature from 25°C will lead to a 0.15 mg/L decrease in DO saturation.

In addition, an increase in water temperature will increase the biological rates including both phytoplankton growth and remineralization of organic substances. As the phytoplankton growth was mostly limited by nutrient limitation, temperature tended to influence remineralization more than phytoplankton growth. Temperature could also affect the pycnocline, which could limit vertical mixing and alter hypoxia in deeper layers. By only changing the stratification under climate warming conditions, the hypoxic volume in the Bay increased from 4.57 to 4.61 $km^3$, an increase of <1%. When the biological rates were computed with the climate warming temperature, the hypoxia volume increased to 4.73 $km^3$, an increase of about 3%. When only the DO saturation was computed with climate warming conditions, the hypoxia volume increased to 4.78 $km^3$, an increase of 5%. Therefore, changes in DO solubility had the highest influence on DO in the deep layers of the Bay due to climate warming, followed by biological rates, whereas changes in the stratification played a minor role. Assuming the total impact on a score of 100%, DO solubility contributed 56%, biological rate changes contributed 33%, and stratification contributed 11%.

Climate warming has the potential to prolong the duration of hypoxia as well. Murphy et al. (2011)

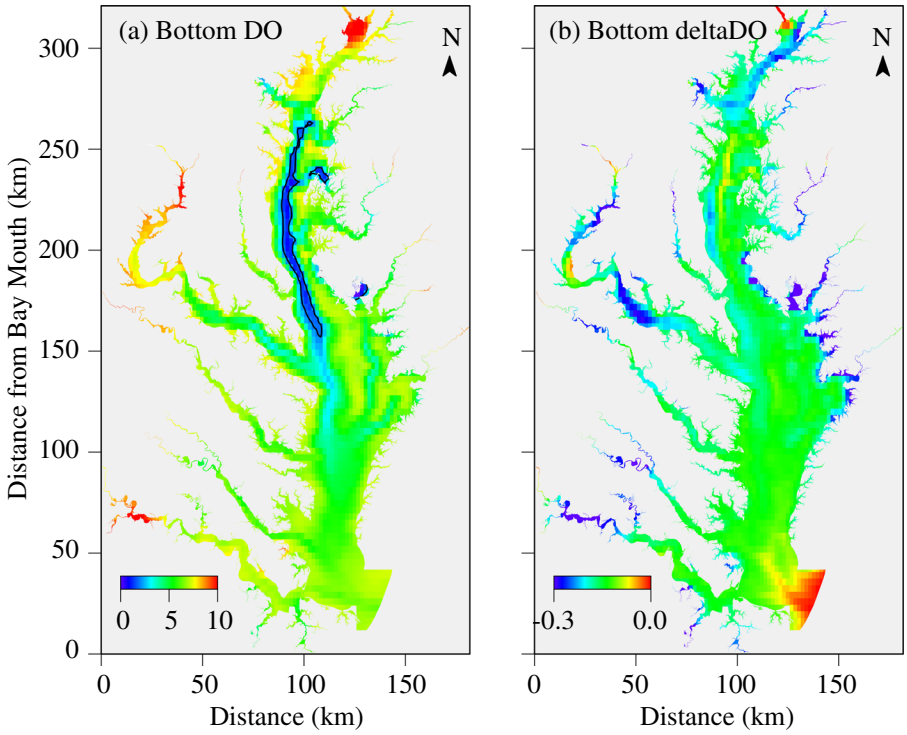


FIGURE 9. Simulated bottom DO (a) and DO change under CWC (b) averaged in August over 10 years (in mg/L).

developed a method to quantify hypoxic duration at an observation station in the deep central Bay. When the daily average DO concentration for the bottom 5 m of the water column is below the critical value of 2 mg/L that day is counted as a hypoxic day. The sum of hypoxic days in a year gives the hypoxia duration. We applied this method to the central station CB4.2C to estimate the impact of climate warming on the duration of hypoxia in the Bay (Figure 10b). The hypoxic duration averaged over the 10 simulation years in the calibration run was 124.8 days, which increased by 6.6% to 133.0 days in the run with all factors combined. Change in DO solubility extended the hypoxia duration from 124.8 to 126.9 days (1.7% increase), biological rates to 127.2 days (1.9% increase), and stratification to 127.3 days (2.0% increase). Note that the sum of the effect of each individual factor was smaller than the effect of all the factors combined due to interaction among the factors.

### *Primary Production, Remineralization, and Sediment Oxygen Demand in the Central Bay Segment CB4MH*

The Chesapeake Bay Program divides the Chesapeake and its tidal tributaries into monitoring segments to organize data collection (USEPA 2004). The segment CB4MH is in the central Bay where annual hypoxia is particularly widespread and persistent. The segment name indicates that it is the fourth main stem monitoring segment (CB4) from the head of the Bay in the mesohaline region (MH). It also has a relatively well-defined boundary without major tributaries (Figure 1). The largest tributary discharging directly to this segment is the Choptank River, with a long-term average discharge of 6 $m^3/s$ (USGS 2020a), which is negligible as compared to the total freshwater discharge in to the Bay of 2,254 $m^3/s$ (USGS 2020b). As such, this segment was used for integrated variable analysis in this paper. The simulated gross primary production in CB4MH was 2.26 g $C/m^2$/day, which is consistent with the literature (Figure 11a). Son et al. (2014) found that CB4MH was a high primary production region, ranging from 1 to 3 g $C/m^2$/day. Harding et al. (2016) reported that net primary production ranged from 1.6 g $C/m^2$/day in dry years to 2.6 g $C/m^2$/day in wet years in Chesapeake Bay. The primary production increased to 2.32 g $C/m^2$/day in the climate warming scenario, an increase of about 3%. Both changes in DO solubility and stratification did not significantly alter the primary production, with an increase of <1% to 2.27 g $C/m^2$/day. Change in the biological rate contributed

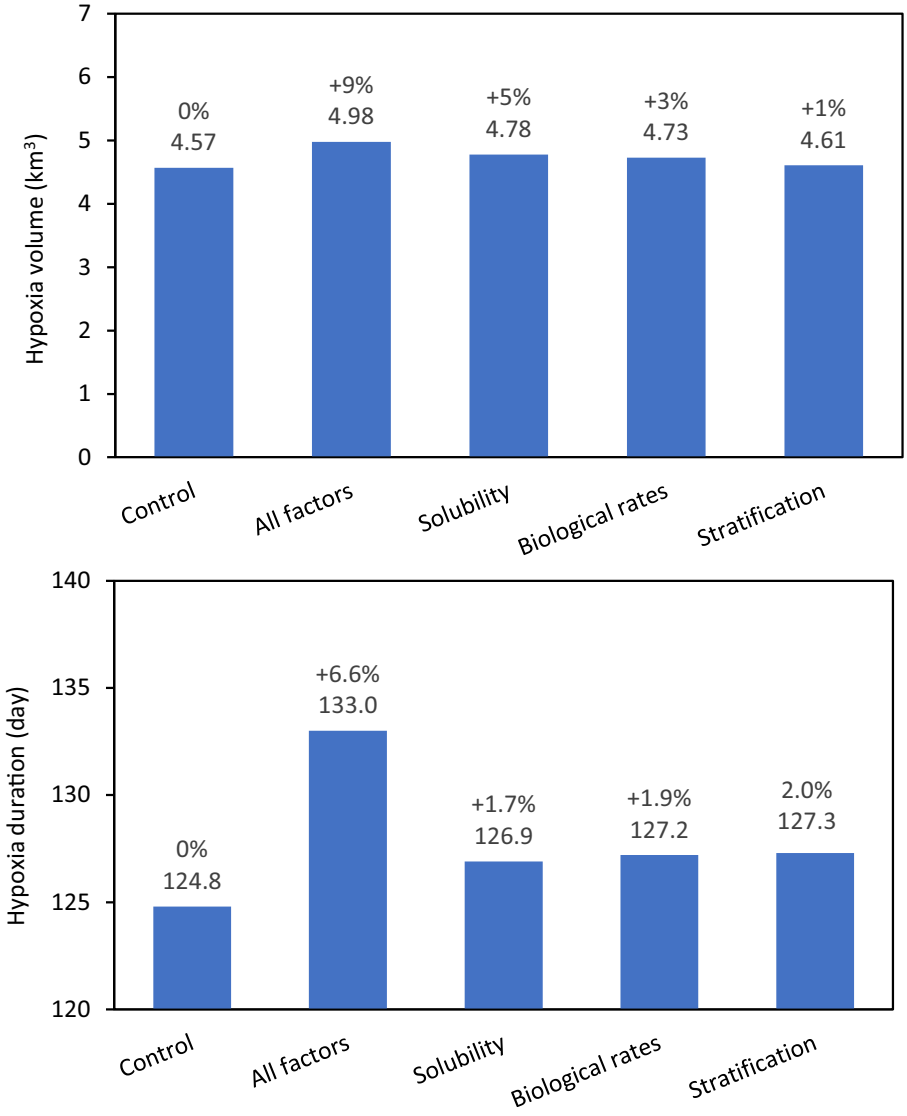


FIGURE 10. (a) Hypoxic volume ($km^3$) in the whole Bay averaged in summer from June through September over 10 years (b) Hypoxic duration (days) at the monitoring station CB4.3C for the entire year, averaged over 10 years of simulation. Control: The control run; All factors: All warming effects; Solubility: The same as the control run but DO solubility computed under CWC; Biological rates: The same as the control run but the biological rates were calculated under CWC; Stratification: The same as the control run but with turbulence diffusivity under CWC. Percentages are the relative changes compared to the control run.

the most to the climate warming impact on primary production, with an increase of 2% to 2.30 g C/$m^2$/day.

The community respiration in the control run was 4.96 g O/$m^2$/day (Figure 11b). With an O:C weight ratio of 2.67, the community respiration was 1.86 g C/$m^2$/day in the control run, amounting to 82% of the primary production. In the scenario under climate warming conditions with all factors combined, the community respiration increased 3.6% to 5.14 g O/$m^2$/day, which is higher than the 3% increase in primary production. Community respiration increased by 2.4% in biological rates scenario, 0.8% in the DO solubility scenario, and 0.4% in the stratification scenario compared to the control run.

Sediment oxygen demand (SOD) was 0.67 g O/$m^2$/day in the control scenario, representing 14% of the community respiration in the water column (Figure 11c). Field measurements of SOD reported by Cowan and Boynton (1996) ranged from 0.05 to 0.86 g O/$m^2$/day, encompassing the simulated value. SOD in the All factors scenario under the climate warming condition increased by 3% to 0.69 g O/$m^2$/day. The biological rate dominated, contributing

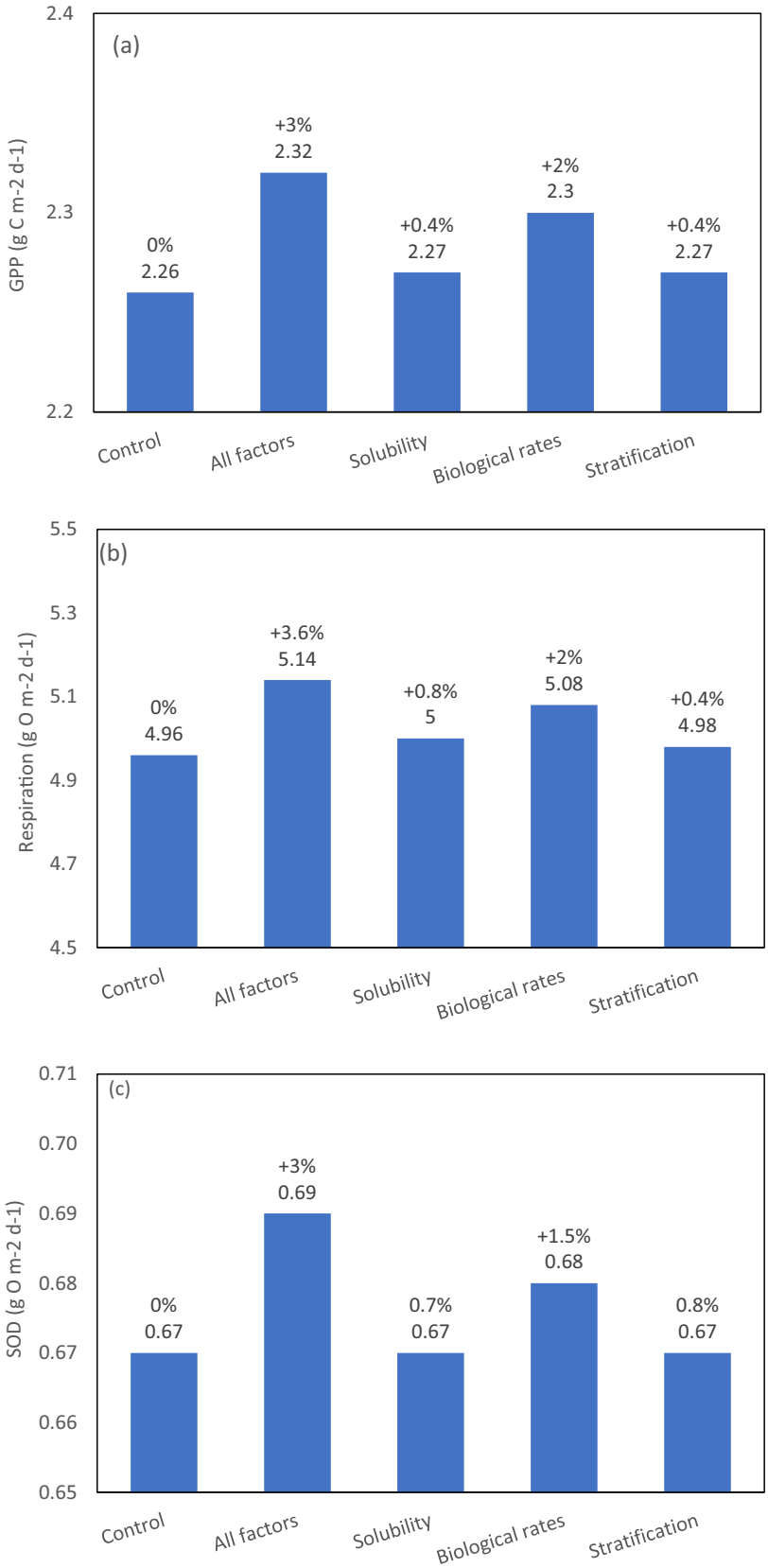


FIGURE 11. Gross primary production (a), community respiration (b), and sediment oxygen demand (c) averaged in summer from June through September over 10 years in the central segment CB4MH of the Bay (see Figure 10 caption for scenario definition). Percentages are the relative changes as compared to the control run.

about 50% of the total effect, whereas the DO solubility and stratification scenarios combined contributed the other 50%.

## DISCUSSION

### *Bottom Water Temperature and Heat Flux*

Bottom water temperatures were similar to the surface layer during the summer season. A key question is: How does heat from the surface reach the bottom? In the model, the heat flux from the atmosphere warms only the surface layer. Theoretically, solar radiation can penetrate the water column to the depth of the euphotic zone. Vertical mixing could bring surface water and associated heat to the bottom. However, given the strong halocline year-round, vertical mixing is limited, particularly during the summer season. An alternative possibility is through horizontal advection. There is a sill in the lower Bay at the mouth of the Rappahannock River, the Rappahannock Shoal, where the water depth of 13 m is considerably shallower than upstream or downstream sections of the Bay. This is known as a hydraulic control point where convergence and downwelling happens (Maryland Sea Grant College 2004; Scully 2016), which has the potential to bring surface water of higher temperature to the deep channel. Scully (2016) conducted a field investigation across the Rappahannock Shoal and found strengthened vertical mixing and downwelling entrainment of surface water to the deep channel. The average salinity distribution across the Rappahannock Shoal in August over the 10-year simulation period shows a frontal convergence zone on the north side of the Rappahannock Shoal (Figure 12a). Salinity increases from 20 to 23 psu over a short distance across the shoal. Low salinity water was entrained from the shoal to the deep channel and this distribution pattern bears high similarity with field observations (Scully 2016).

Water temperature is higher in the deeper layers to the north of the Shoal compared to the deeper layers south of the shoal and shows a decreasing trend northward into the Bay, from about 25°C to 24°C (Figure 12b). Temperature isopleths sloped downward similarly to the salinity isopleths, supporting the interpretation that surface water from the shoals was entrained into the deeper Bay. Scully (2016) found that the water mass entrained in the deep channel propagates up-estuary to the mid-Bay along the deep channel and that this mechanism leads to a water temperature increase in the deep channel of the Bay. As mentioned

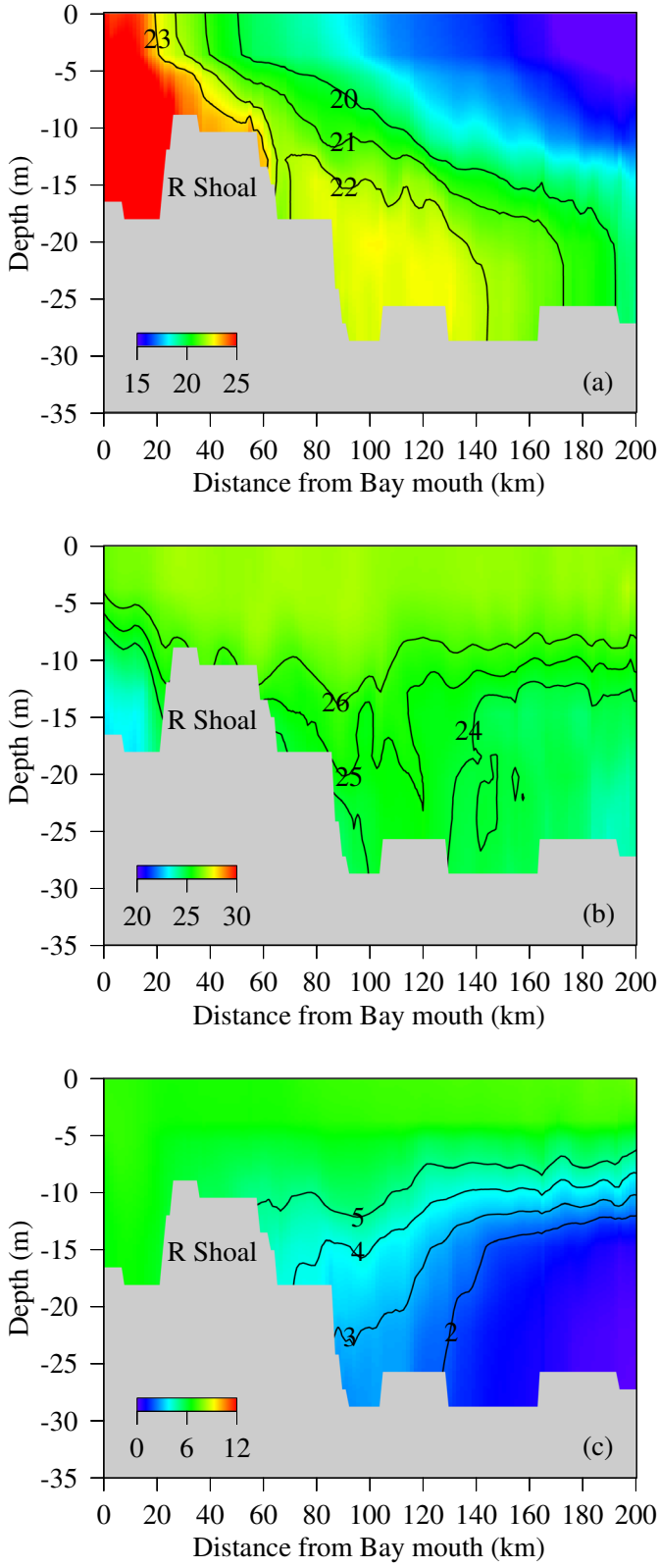


FIGURE 12. Salinity (a), temperature (b), and DO (c) transects along the main stem from the Bay mouth, crossing the Rappahannock Shoal (R Shoal) to the central Bay, average in August over the 10 simulated years in the control run.

earlier, the increase in water temperature in the deep channel lags the surface water by about four weeks during the spring season at the central station CB4.2C. In fact, this lag time increases from the Rappahannock Shoal to the upper Bay (Figure 13). At Station CB6.1 on the Shoal, surface and bottom water temperature increases almost simultaneously during spring. At Station CB5.2 in the lower middle Bay, there is a lag time between surface and bottom water temperature on the order of two weeks. At the central station CB4.2C, the lag time increases to about four weeks and at the station CB3.3C in the upper Bay, the lag time increases further to about six weeks. This gradual increase in temperature lag time from the Rappahannock Shoal to the upper Bay is coherent with the fact that water of higher temperature is entrained from the Shoal to the deep channel and then propagates upstream along the deep channel. The distance from the Shoal to the central monitoring station CB4.2C is about 107 km. Propagation of 107 km in four weeks necessitates a speed of water mass movement of about 0.04 m/s. A propagation speed of 0.08 m/s was estimated from field measurements (Scully 2016). The propagation speed can vary in response to forcing like wind events or freshwater discharges, which affect the intensity of convergence and water mass entrainment in the vicinity of the Shoal.

### *Climate Warming Impact on Bottom DO and Hypoxia*

A rapid drop in bottom DO occurred when bottom temperature increased to about 15°C, which corresponds to an abrupt decrease in bottom organic matter as indicated by chlorophyll concentration. The winter bottom temperature was about 5°C and an increase to 15°C doubled the respiration and remineralization rate, which appeared to be the primary driver for hypoxia development in the deep Bay. Remineralization and sediment early diagenesis are accelerated under increased water temperature leading to increased oxygen consumption as reflected in the biological rate scenario compared with the control scenario.

The effect of DO solubility on hypoxia development is stronger than either the biological rate or stratification effect. A DO anomaly is generated when relatively high DO water extends to the deeper layers near the Rappahannock Shoal (Figure 12c), following the same pattern as salinity and temperature. In the control scenario, this constitutes a source of DO to the deep channel (Scully 2016). With climate warming, the entrained water will have relatively lower DO due to saturation effects, reducing the DO supply through vertical mixing and convection at the Rappahannock hydraulic control point. The subpycnocline upstream DO flux at the southern boundary of the central segment CB4MH was 16.0 kg/s into the segment and 11.9 kg/s through the northern boundary out of the segment in the control scenario in summer (June–September). Given that the total volume below the surface pycnocline is about $4.88 \times 10^9$ m$^3$, the horizontal flux would increase DO concentration by 0.073 mg/L per day on average if DO consumption remained the same. The reduced solubility lowered

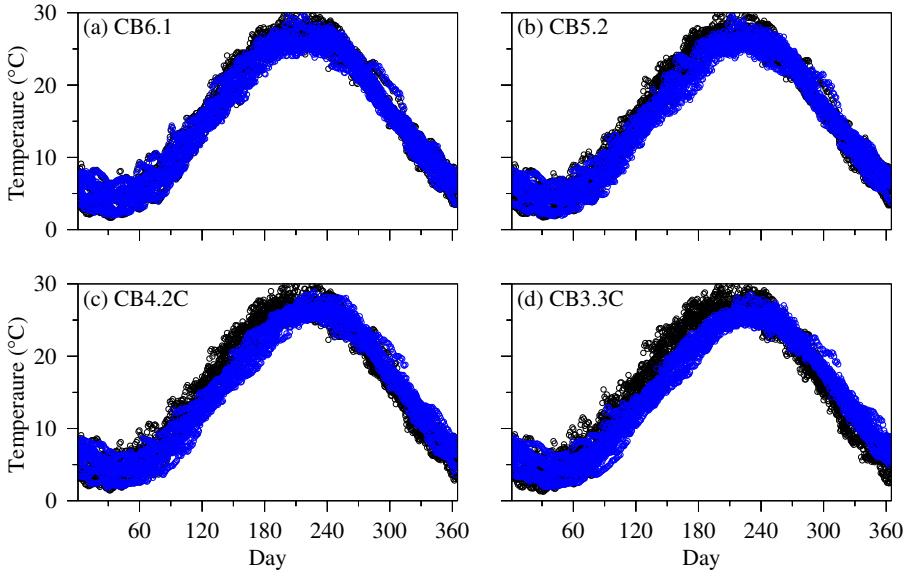


FIGURE 13. Increasing lag time between the bottom (blue) and surface (black) temperature increase during spring over the 10-year ensemble simulation from the lower Bay station CB6.1 (a) on the Rappahannock Shoal to the upper Bay station CB3.3C (d) in the control run (Lag time increased from negligible at Station CB6.1 (a) to two weeks at Station CB5.2 (b), four weeks at Station CB4.2C (c), and six weeks at Station CB3.3C) (d), reflected by the increasing shift between the black and blue circles, with each color representing 10-year ensemble simulation.

the horizontal DO flux crossing the boundaries of segment CB4MH. The DO flux crossing the southern boundary decreased by 3% to 15.5 kg/s and at the northern boundary also by 3% to 11.5 kg/s, leading to a daily change of 0.071 mg/L in DO concentration, lower than in the control run.

Climate change has multiple ways of affecting water quality in the Bay, such as changes in precipitation, nutrient loadings from the watershed, and sea level rise. This paper focuses only on climate warming effects. Effects of climate change on precipitation and nutrient loadings from the watershed are covered in Bhatt et al. (this volume) and the influence of sea level rise on Chesapeake water quality is described in Linker et al. (this volume). The simulation projected changes over 30 years from 1995 to 2025.

## CONCLUSION

Under the ever-increasing climate warming impact on estuarine and aquatic ecosystems, understanding the mechanisms through which climate change alters the functionality of ecosystems and influences water quality is critical for effective adaptive management decision making to mitigate climate warming impacts. Chesapeake Bay, the largest estuary in the U.S., is under severe anthropogenic stress from excessive nutrient loadings leading to eutrophication and hypoxia in the summer. A large-scale, comprehensive partnership, the Chesapeake Bay Program, is working to mitigate the anthropogenic stress by reducing nutrient loadings from the watershed under the Chesapeake TMDL, established in 2010 (USEPA 2010). The 2010 TMDL and subsequent management decisions were made assuming 1991–2000 climate conditions. It is critical, however, to assess the management decisions and measures under future climate change conditions to guide adaptive management actions and ensure the effectiveness and success of the management program.

The regulatory model suite of CH3D-ICM has been used in this paper to assess climate warming impacts on water quality as measured by DO concentration and hypoxic volume in Chesapeake Bay. The model has been first calibrated with field observations from 1991 to 2000, and then applied under climate warming conditions. Further model application allowed us to discern the impact of individual factors related to climate warming, including changes in DO solubility, biological rate, and stratification. Bottom water temperature increases during later spring and earlier summer accelerate remineralization and set up hypoxia development in the deep channel. Climate warming alters the biogeochemical dynamics through changes in DO solubility, remineralization rate, and stratification. Model simulation estimates that climate warming by 1.06°C in the atmosphere from 1995 to 2025 will lead to an increase of about 0.90°C in water temperatures in the surface layers of the Bay and about 0.85°C in the deeper central Bay. The water temperature change will lead to an increase in summer hypoxia volume of 9% in the entire Bay (410 $Mm^3$), of which change in DO solubility will contribute 56%, changes in biological rates 33%, and stratification 11%. The effect of changes in biological rates is readily understandable. Primary production, respiration, remineralization, and SOD all increase under climate warming conditions. Likewise, the stratification effect increases under climate warming leading to a decrease in vertical mixing. However, the effect of changes in DO solubility, which is the primary factor in determining the climate warming effect on DO, requires a more nuanced explanation since hypoxic water oxygen content is not directly limited by solubility. It has been found that the Rappahannock Shoal, a hydraulic control spot, plays a critical role in controlling bottom water temperature and DO flux in the deep channel of the Bay. The abrupt change in bathymetry from the deep channel to the Rappahannock Shoal creates a convergence zone between fresher southward-moving surface water and saltier northward-moving bottom water from the coastal ocean, where downwelling and enhanced vertical mixing occur. The water of higher temperature entrained from the Rappahannock Shoal into the deep channel propagates upstream to the central Bay, accelerates the remineralization of organic matter, and thus leads to rapid development of hypoxia in the deep channel. Under climate warming conditions, the DO saturation and DO concentration on the Rappahannock Shoal decrease, reducing the DO flux entrained to the deep channel and leading to an increase in hypoxic volume stemming from changes in DO solubility. Our findings add another dimension to the understanding of the formation and climate warming impact on hypoxia in the Bay.

## ACKNOWLEDGMENTS

The authors thank the Chesapeake Bay Program and UMCES IAN to provide data and funding (CB-75230480) for this project, the Maryland Department of Natural Resource to provide observation data and three anonymous reviewers for their constructive comments. Special thanks go to Bill Dennison and Dave Nemazie for their guidance and help. Any use of trade, firm, or product names is for descriptive purposes only and does not imply endorsement by the U.S. Government.

## AUTHORS' CONTRIBUTIONS

**Richard Tian:** Conceptualization; data curation; formal analysis; funding acquisition; investigation; methodology; resources; software; supervision; validation; visualization; writing-original draft; writing-review & editing. **Carl F. Cerco:** Formal analysis; investigation; methodology; software; supervision; validation; writing-original draft; writing-review & editing. **Gopal Bhatt:** Conceptualization; data curation; formal analysis; investigation; methodology; software; validation; writing-review & editing. **Lewis C. Linker:** Conceptualization; data curation; formal analysis; funding acquisition; investigation; methodology; project administration; resources; supervision; validation; writing-review & editing. **Gary W. Shenk:** Conceptualization; data curation; formal analysis; funding acquisition; investigation; methodology; project administration; resources; supervision; writing-review & editing.

## LITERATURE CITED


Altieri, A.H., and K.B. Gedan. 2015. "Climate Change and Dead Zones." *Global Change Biology* 21: 1395–406.

Bhatt, G., L. Linker, G.W. Shenk, R. Tian, I. Bertani, P. Claggett, J. Rigelman, and K. Hinson. This volume. "Water Quality Impacts of Land Use, Growth, and Climate Change in the Midpoint Assessment of the Chesapeake Bay TMDL." *Journal of the American Water Resources Association*.

Cerco, C., and T. Cole. 1993. "Three-Dimensional Eutrophication Model of Chesapeake Bay." *Journal of Environmental Engineering* 119: 1006–25.

Cerco, C.F., and M.R. Noel. 2004. "The 2002 Chesapeake Bay Eutrophication Model." USEPA Report, EPA 903-R-04-004, 374 pp.

Cerco, C.F., and M.R. Noel. 2013. "Twenty-One-Year Simulation of Chesapeake Bay Water Quality Using the CE-QUAL-ICM Eutrophication Model." *Journal of the American Water Resources Association* 49: 1119–33.

Chesapeake Bay Program. 2017. "Chesapeake Assessment and Scenario Tool (CAST) Version 2017d." Chesapeake Bay Program Office. https://cast.chesapeakebay.net/Documentation/ModelDocumentation.

Chesapeake Bay Program. 2020. "Chesapeake Bay Program Climate Change Analysis Documentation of Methods and Decisions for 2019–2021 Process." Chesapeake Bay Program Office. https://cast.chesapeakebay.net/Documentation/ModelDocumentation.

Cowan, J.L.W., and W.R. Boynton. 1996. "Sediment-Water Oxygen and Nutrient Exchanges along the Longitudinal Axis of Chesapeake Bay: Seasonal Patterns, Controlling Factors and Ecological Significance." *Estuaries* 19: 562–80.

Diaz, R.J., and D.L. Breitburg. 2009. "The Hypoxic Environment." *Fish Physiology* 27: 1–23.

DiToro, D., and J. Fitzpatrick. 1993. "Chesapeake Bay Sediment Flux Model." Contract Report EL-93-2, US Army Engineer Waterways Experiment Station, Vicksburg, MS, 200 pp.

Du, J.L., J. Shen, K. Park, Y.P. Wang, and X. Yu 2018. "Worsened Physical Condition Due to Climate Change Contributes to the Increasing Hypoxia in Chesapeake Bay." *Science of the Total Environment* 630: 707–17.

Dupigny-Giroux, L.A., E.L. Mercay, M.D. Lemcke-Stampone, G.A. Hodgkins, E.E. Lentz, K.E. Mills, E.D. Lane et al. 2018. "Northeast." In *Impacts, Risks and Adaptation in the United States: Forth National Climate Assessment* (Volume II), edited by D.R. Reidmiller, C.W. Avery, D.R. Easterling, K.E. Kunkel, K.L.M. Lewis, T.K. Maycock, and B.C. Stewart. Washington, D.C.: U.S. Global Change Research Program. https://doi.org/10.7930/NCA4.2018.CH18.

Edinger, J., D. Brady, and J. Geyer. 1974. "Heat Exchange and Transport in the Environment." Report 14, Department of Geography and Environmental Engineering, Johns Hopkins University, Baltimore, MD.

Garcia, H.E., and L.I. Gordon. 1992. "Oxygen Solubility in Seawater: Better Fitting Equations." *Limnology and Oceanography* 37: 1307–12.

Harding Jr., L.W., M.E. Mallonnee, E.S. Elgin, W.D. Miller, J.E. Adolf, C.L. Gallogos, and H.W. Paerl. 2016. "Variable Climatic Conditions Dominate Recent Phytoplankton Dynamics in Chesapeake Bay." *Nature*. https://doi.org/10.1038/srep23773.

IPCC. 2013. "Summary for Policymakers." In *Climate Change 2013: The Physical Science Basis. Contribution of Working Group I to the Fifth Assessment Report of the Intergovernmental Panel on Climate Change*, edited by T.F. Stocker, D. Qin, G.K. Plattner, M. Tignor, S.K. Allen, J. Boschung, A. Nauels, Y. Xia, V. Bex, and P.M. Midgley, 3–29.Cambridge, United Kingdom and New York, NY: Cambridge University Press.

Irby, I.D., M.A.M. Friedrichs, D. Fei, and K.E. Hinson. 2018. "The Competing Impacts of Climate Change and Nutrient Reductions on Dissolved Oxygen in Chesapeake Bay." *Biogeosciences* 15: 2649–68.

Johnson, B.H., K.W. Kim, R.E. Heath, H.L. Butler, and B.B. Hsieh. 1991. "User's Guide for a Three-Dimensional Numerical Hydrodynamic, Salinity, and Temperature Model of Chesapeake Bay." US Army Corps of Engineers, Technical Report HL-91-20, 82 pp.

Jolliff, J.K., J.C. Kindle, I. Shulman, B. Penta, M.A.M. Friedrichs, R. Helber, and R.A. Arnone. 2009. "Summary Diagrams for Coupled Hydrodynamic-Ecosystem Model Skill Assessment." *Journal of Marine Systems* 76: 64–82.

Justic, D., N.N. Rabalais, and R.E. Turner. 1997. "Impacts of Climate Change on Net Productivity of Coastal Waters: Implications for Carbon Budgets and Hypoxia." *Climate Research* 8: 225–37.

Lehrter, C., D.S. Ko, L.L. Lowe, and B. Penta. 2017. "Predicted Effects of Climate Change on Northern Gulf of Mexico Hypoxia." *Modeling Coastal Hypoxia*, edited by D. Hypoxia, K.A. Justic, R.D. Hetland, and K. Fennel, 173–214.Cham: Springer.

Li, Y., M. Li, and W.M. Kemp. 2015. "A Budget Analysis of Bottom-Water Dissolved Oxygen in Chesapeake Bay." *Estuaries and Coasts*. https://doi.org/10.1007/s12237-014-9928-9.

Linker, L.C., R.A. Batiuk, G.W. Shenk, and C.F. Cerco. 2013. "Development of the Chesapeake Bay Watershed Total Maximum Load Allocation." *Journal of the American Water Resource Association* 49: 986–1006.

Linker, L.C., G. Bhatt, R. Tian, G.W. Shenk, and C.F. Cerco. This volume. "Climate Change Risk to Chesapeake Water Quality and Implications for the Chesapeake TMDL." *Journal of the American Water Resources Association*.

Maryland Sea Grant College. 2004. "The Hydraulics of a Hot Spot." *Chesapeake Quarterly* 3: 8–12.

Meire, L., K.E.R. Soetaert, and F.J.R. Meysman. 2013. "Impact of Global Change on Coastal Oxygen Dynamics and Risk of Hypoxia." *Biogeosciences* 10: 2633–53.

Murphy, L., W.M. Kemp, and W.P. Ball. 2011. "Long-Term Trends in Chesapeake Bay Seasonal Hypoxia, Stratification, and Nutrient Loading." *Estuaries and Coasts* 34: 1293–309.

Najjar, R.G., C.R. Pyke, M.B. Adams, D. Breitburg, C. Hershner, M. Kemp, R. Howarth et al. 2010. "Potential Climate Change Impacts on the Chesapeake Bay." *Estuarine, Coastal and Shelf Science* 86: 1–20.

Preston, B.L. 2004. "Observed Winter Warming of the Chesapeake Bay Estuary (1949–2002): Implications for Ecosystem Management." *Environmental Management* 34: 125–39.

Roman, M.R., S.B. Brandt, E.D. House, and J.J. Pierson. 2019. "Interactive Effects of Hypoxia and Temperature on Coastal Pelagic Zooplankton and Fish." *Frontier in Marine Science*. https://doi.org/10.3389/fmars.2019.00139.

Scully, M.E. 2016. "Mixing of Dissolved Oxygen in Chesapeake Bay Driven by the Interaction between Wind-driven Circulation and Estuarine Bathymetry." *Journal of Geophysical Research Oceans* 121: 5639–54.

Sheng, Y.P. 1990. "Evolution of a Three-Dimensional Curvilinear-Grid Hydrodynamic Model for Estuaries, Lakes and Coastal Waters: CH3D." In *Estuarine and Coastal Modeling*, edited by M.L. Spaulding, 40–49.Reston, VA: ASCE.

Sheng, Y.P., D.E. Eliason, X.J. Chen, and J.K. Choi. 1991. "A Three-Dimensional Numerical Model of Hydrodynamics and Sediment Transport in Lakes and Estuaries: Theory, Model Development, and Documentation." Final Report for Environmental Research Laboratory, U.S.E.P.A., Athens, GA, 326 pp.

Sheng, Y.P., and J.E. Hirsh. 1984. "Numerical Solution of Shallow Water Equations in Boundary Fitted Grid." Tech. Memo 84-15, Aeronautical Research Associates of Princeton, Princeton, NJ.

Son, S.H., M.H. Wang, and L.W. Harding Jr. 2014. "Satellite-Measured Net Primary Production in the Chesapeake Bay." *Remote Sensing of Environment* 144: 109–19.

Taylor, K.E. 2001. "Summarizing Multiple Aspects of Model Performance in a Single Diagram." *Journal of Geophysical Research* 106: 7183–92.

Taylor, K.E., R.J. Stouffer, and G.A. Meehl. 2011. "An Overview of CMIP5 and the Experiment Design." *Bulletin of the American Meteorological Society* 93 (4): 485–98. https://doi.org/10.1175/BAMS-D-11-00094.1.

Thomas, A.C., A.J. Pershing, K.D. Friedland, J.A. Nye, K.E. Mills, M.A. Alexander, N.R. Record, R. Weatherbee, and M.E. Henderson. 2017. "Seasonal Trends and Phenology Shifts in Sea Surface Temperature on the North American Northeastern Continental Shelf." *Elementa: Science of the Anthropocene* 5: 48. https://doi.org/10.1525/elementa.240

Tian, R. 2019. "Factors Controlling Saltwater Intrusion Across Multi-time Scales in Estuaries, Chester River, Chesapeake Bay." *Estuarine, Coastal and Shelf Science* 223: 61–73.

Tian, R., C. Chen, J. Qi, R. Ji, R.C. Beardsley, and C. Davis. 2014. "Modeling Study of Nutrient and Phytoplankton Dynamics in the Gulf of Maine: Patterns and Drivers for Seasonal and Interannual Variability." *ICES Journal of Marine Science*. https://doi.org/10.1093/icesjms/fsu090.

USEPA (U.S. Environmental Protection Agency). 2004. *Chesapeake Bay Program Analytical Segmentation Scheme: Revisions, Decisions and Rationales 1983–2003*. Annapolis, MD: U.S. Environmental Protection Agency, Region 3, Chesapeake Bay Program Office.

USEPA. 2010. *Chesapeake Bay Total Maximum Daily Load for Nitrogen, Phosphorus and Sediment*. Annapolis, MD: U.S. Environmental Protection Agency Chesapeake Bay Program Office. http://www.epa.gov/reg3wapd/tmdl/ChesapeakeBay/tmdlexec.html.

USGS. 2020a. "USGS 01491000 Choptank River Near Greensbord, MD." https://waterdata.usgs.gov/usa/nwis/uv?01491000.

USGS. 2020b. "Freshwater Flow into Chesapeake Bay." https://www.usgs.gov/centers/cba/science/freshwater-flow-chesapeake-bay?qt-science_center_objects=1#qtscience_center_objects.

Westrich, J., and R. Berner. 1984. "The Role of Sedimentary Organic Matter in Bacterial Sulfate Reduction: The G model tested." *Limnology and Oceanography* 29: 236–49.

Xia, M., and L. Jiang. 2016. "Application of an Unstructured Grid-Based Water Quality Model to Chesapeake Bay and Its Adjacent Coastal Ocean." *Journal of Marine Science and Engineering* 4 (52): 1–23.

Zhang, J., D. Gilbert, A.J. Gooday, L. Levin, and S.W.A. Naqvi. 2010. "Natural and Human-Induced Hypoxia and Consequences for Coastal Areas: Synthesis and Future Development." *Biogeosciences* 7: 1443–67.

Zhong, L., and M. Li. 2006. "Tidal Energy Fluxes and Dissipation in the Chesapeake Bay." *Continental Shelf Research* 26: 752–70.